Vortex packets and the structure of wall turbulence

R.J. Adrian[1] and S. Balachandar[2]
Department of Theoretical and Applied Mechanics, University of Illinois at Urbana-Champaign
216, 61801 Talbot Lab, Urbana, IL.
e-mail:[1] *r-adrian@uiuc.edu;* [2] *s-bala@uiuc.edu*

Recibido el 9 de septiembre de 1999; aceptado el 24 de septiembre de 1999

Experimental evidence in low to moderate Reynolds number wall flows shows that hairpin vortices (including asymmetric inclined vortices) occur in groups that propagate as a whole with relatively slow dispersion. These groups, or "packets", grow upwards from the buffer layer to about one-half of the thickness of the boundary layer. Direct numerical simulations of the growth of a single hairpin eddy in a clean background flow show how these packets may be formed in the near wall (low Reynolds number) region by a viscous autogeneration mechanism that is similar in many regards to the mechanism proposed by Smith *et al.* [*Philos. Trans. R. Soc. London, Ser. A* **336** (1991) 131]. The organization of hairpin eddies into packets and the interactions of those packets is an important feature of wall turbulence that provides a new paradigm by which many seemingly unconnected aspects of wall turbulence can be explained. These include the inordinately large amount of streamwise kinetic energy that resides in very long streamwise wavelengths, the occurrence of multiple Q2 events per turbulent burst, the formation of new streamwise vorticity, and the characteristic angles of inclination of fronts. The autogeneration process may also explain the formation of long quasi-streamwise vortices in the buffer layer and the associated low-speed streaks.

Keywords: Vortex packets; low Reynolds number

Evidencia experimental en la región de baja a moderada del número de Reynolds en flujos de pared muestra que vórtices (incluyendo vórtices asimétricos inclinados) ocurren en grupos que se propagan como un todo con dispersión relativamente baja. Estos grupos, o "paquetes", crecen a partir de la capa basal a cerca de la mitad del espesor de la capa limítrofe. Simulaciones numéricas directas del crecimiento de un solo remolino en un flujo circundante limpio muestran como estos paquetes pueden formarse en la región cercana a una pared (bajo número de Reynolds) por un mecanismo de autogeneración viscosa que es similar en muchos aspectos al mecanismo propuesto por Smith *et al.* [*Philos. Trans. R. Soc. London, Ser. A* **336** (1991) 131]. La organización de remolinos en paquetes y la interacción de esos paquetes es un hecho importante de turbulencia de paredes que proveé un nuevo paradigma por el cual muchos aspectos aparentemente no conectados de turbulencia de paredes pueden ser explicados. Éstos incluyen la gran cantidad no ordinaria de energía cinética de torrentes que reside en longitudes de onda de torrentes grandes, la ocurrencia de múltiples eventos Q2 por ocurrencia de turbulencia, la formación de nueva vorticidad torrencial, y los ángulos característicos de inclinación de frentes. El proceso de autogeneración puede explicar también la formación de grandes vórtices quasi-torrenciales en la capa basal y las líneas asociadas de baja velocidad.

Descriptores: Paquetes de vórtices; bajo número de Reynolds

PACS: 47.32.-y; 47.27.-i

1. Introduction

Hairpin shaped vortices are thought by many to be a central feature of turbulent wall layers. An idealized hairpin vortex consists of a pair of counter-rotating quasi-streamwise vortices that are tilted upwards along the downstream direction and a hairpin head that connects to the quasi-streamwise vortices at their downstream ends, as shown in Fig. 1. Hairpin vortices observed in experiments and computations seldom possess perfect spanwise symmetry; more often they are asymmetric, left- or right-handed cane-like vortices, which consist of a head, a neck and one dominant quasi-streamwise leg [1, 2]. Nevertheless, a picture of the turbulent wall layer as a distribution of hairpin vortices provides a reasonable model for many of the flow features that have been observed and documented in the past (*c.f.* Ref. 4 for example).

In the streamwise wall normal xy plane, the velocity signature of a hairpin vortex is characterized by a circular vortex core and a strong outward pumping of low momentum fluid.

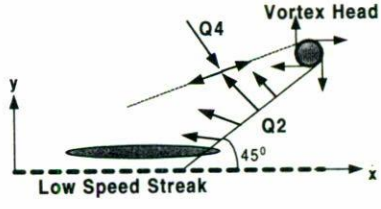

FIGURE 1. Schematic of a hairpin vortex and associated flow field properties that form the signature of a hairpin on the xy plane.

This hairpin vortex signature is relatively insensitive to the degree of asymmetry of the hairpin. Recent PIV measurements [4–6] in a turbulent boundary layer over a range of Reynolds numbers clearly show numerous hairpin vortex signatures within the boundary layer, providing strong evidence that the turbulent wall layer at moderate Reynolds numbers is thickly populated with hairpin vortices.

In the experimental measurements cited above the hairpin vortices were often observed to occur one behind the other as

a train in the streamwise direction forming a coherent group or packet of hairpin vortices. Although the shapes and sizes of the packet varied, the tendency to form group of hairpins was observed at all instances. The streamwise coherence of the near-wall hairpin vortices persisted even at higher Reynolds numbers. The hairpin vortices within a packet were observed to work cooperatively passing low-speed fluid from the downstream most vortex to its upstream neighbor and so on over several hairpin vortices to form a low-speed streak of length significantly longer than a single hairpin vortex. As a result, transport properties, such as Reynolds stresses, of the packet could significantly exceed a simple sum of the contribution from each individual hairpin within the packet. Thus the arrangement of hairpin vortices into packets with definite distribution of size, age and spatial separation has a potentially large effect on the overall momentum and heat transport from the wall. For instance, significant drag reduction can be anticipated by disturbing the streamwise alignment of hairpins within a packet.

The present paper will focus on the following issues: *a*) A brief review of all experimental evidence supporting the existence of hairpins; *b*) a review of computational results on the autogeneration of new hairpin vortices; *c*) explanation on the basis of the hairpin packet paradigm of experimental observations that cannot be explained by single hairpin models; *d)* the implications of hairpins occurring as packets, instead of being randomly scattered throughout the boundary layer.

Hairpin vortices have a long history. Theodorsen [7] was the first to suggest the importance of hairpin-type vortices in turbulent wall layers. His original proposal consisted of horseshoe vortices with omega-shaped head and neck region that extended spanwise to form spanwise vortex legs.

The visualization experiments of Head and Bandyopadhyay [8] inferred that stretched vortex loops (or hairpin vortices) inclined at about 45° are a major component of the turbulent wall layer. There are two major pieces of experimental evidence showing that hairpins occur in groups. First, the side view smoke flow visualizations of Head and Bandyophadhyay [8] revealed large scale structures, inclined at a characteristic angle of about 20°, that marked the outer edge of the turbulent boundary layer. They inferred that this structure was a group of individual hairpin vortices, each stretching from the wall to the outer edge of the boundary layer, Fig. 2a. (See also the model of Bandyopadhyay [9]) The angle of envelope of the group was approximately 18°. Second, based on experimental observations of hydrogen bubble pattern in the near-wall region of a low Reynolds number turbulent boundary layer, Smith [10] reported that the results are consistent with at least three hairpin vortices forming with alignment along the streamwise direction (near-wall region of Fig. 2b). Subsequent work by Smith and coworkers demonstrated the formation of sequences of hairpins by a stationary hemispherical bump on the wall [11, 12] and by impulsive injection of fluid [13] in a laminar boundary layer. More recent direct numerical simulations by Zhou, Adrian, and Balachandar [14] and Zhou, Adrian, Balachandar, and Kendall [15] on the evolution of a single initial hairpin vortex in a unidirectional mean turbulent channel flow have identified the mechanistic details behind the autogeneration of secondary hairpin vortices in the near-wall region leading to the formation of a hairpin packet. A significant outcome of these simulations is that new hairpins are formed both on the upstream and downstream sides of the initial hairpin resulting in a half-diamond or tent-like hairpin packet. This shape for the hairpin packet is consistent with recent experimental measurements [6] schematically represented in Fig. 2b. The computations also show that the autogeneration process is robust and occurs more readily in the case of an asymmetric initial hairpin, eventually forming a staggered array of one-sided hairpin vortices. This is in accordance with the predominantly one-sided hairpins noted by Guezennec and Choi [1] and Robinson [2].

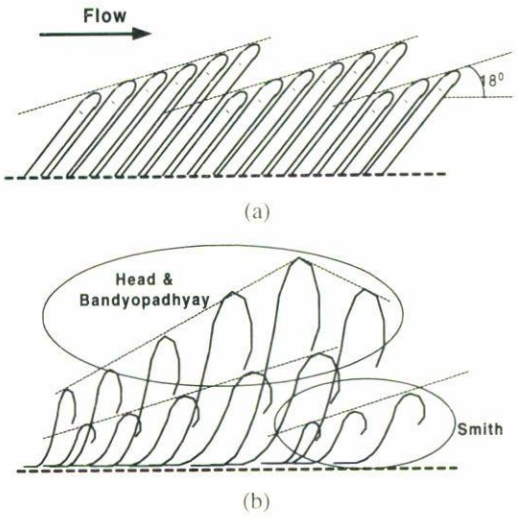

FIGURE 2. Hairpin packet models. (a) Head and Bandyopadhyay [8]; (b) Hierarchy of packets as observed in Ref. 6.

2. Experimental evidence for packets

The velocity signature of a hairpin vortex in a spanwise-wall normal yz plane passing through the quasi-streamwise vortex legs is characterized by a pair of counter rotating vortices pumping fluid away from the wall. On the other hand, in a streamwise-wall normal xy plane the hairpin vortex is characterized by *a*) a strong outward pumping of low momentum fluid on the in-board side of the quasi-streamwise vortices. This quadrant-two (Q2) flow encounters the high-speed freestream and forms a shear layer which is inclined 45° to the horizontal; and *b*) closed/spiraling streamlines corresponding to the circular vortex core of the hairpin head in a frame of reference traveling downstream with the hairpin vortex.

The schematic shown in Fig. 1 clearly illustrates the typical hairpin vortex signature in the xy plane, provided it passes between the quasi-streamwise legs. However, it must be emphasized that this hairpin signature is relatively insensitive to the degree of asymmetry of the hairpin. The hairpin vortex

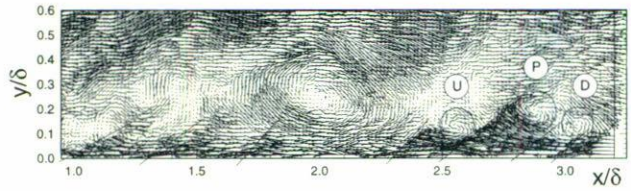

(a)

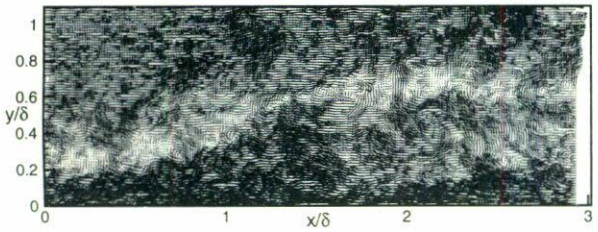

(b)

FIGURE 3. PIV measurements of instantaneous velocity fields in the xy plane of a turbulent boundary layer. (a) $\mathrm{Re}_\theta = 1015$; (b) $\mathrm{Re}_\theta = 7705$.

signature will then allow reasonably accurate identification of hairpin vortices from quantitative measurement of the velocity field within the turbulent wall layer. It should be emphasized that the Q2 vectors exhibit a maximum somewhere below the vortex head and that it is characteristic of the combined induction associated with the proximity of the vortex head and legs. This peak in the Q2 velocity provides a clear evidence for the existence of a three-dimensional vortex, as a two-dimensional vortex, such as a vortex line, is in general incapable of generating such a local velocity maximum.

Figure 3a shows a velocity vector plot in the streamwise-wall normal xy plane obtained from high resolution PIV measurement of a zero pressure gradient boundary layer with $\mathrm{Re}_\theta = 1015$ [6]. A constant convection velocity of $U_c = 0.91\,U_\infty$ (U_∞ is the free stream velocity) has been subtracted from the streamwise velocity in order to bring out the packet of hairpins, whose heads are clearly identified in the figure. The hairpins within the packet are observed to extend from the wall up to $y/\delta \approx 0.5$ to 0.6, where δ defines the edge of the boundary layer. From the convection velocity it can be inferred that the hairpin packet propagates along the streamwise direction at 0.6 to $0.9\,U_\infty$. The PIV measurements cover a wide streamwise range of up to $3.0\,\delta$ and over this extended streamwise range Tomkins [6] observed different geometric shapes for the hairpin packet including: uninterrupted streamwise growth, sawtooth shape, half-diamond or tent shape and constant height. Fig. 3a might fit the description of a packet of constant height. In the case a ramp-like envelope for the hairpin packet, as in uninterrupted growth, sawtooth and half-diamond shape, the mean angle of the ramp is observed to be about 15°, which is consistent with earlier observations of Head and Bandyopadhyay [8]. Furthermore, over the Reynolds number (Re_θ) range form 1000 to 7705, the packet is observed to contain from about 4 hairpins to as many as nine hairpins.

The cooperative action of the streamwise aligned hairpins within the packet can be clearly observed in Fig. 3a as the zone of strong negative velocity that lies below the hairpin vortex heads. This zone of low momentum also exists at higher Reynolds numbers, as shown in Fig. 3b for $\mathrm{Re}_\infty = 7705$ but is restricted closer to the wall in terms of outer units. At higher Reynolds number multiple zones of almost uniform momentum can be observed [4, 5]. The interface between any two adjacent zones is marked by a sequence of vortex cores, which contributes to the near uniform velocity jump across them. These vortex cores can be identified as the heads of nearly streamwise aligned hairpin vortices and thus the interface between the different uniform momentum zones can be interpreted as the envelop of a hierarchical hairpin packet.

The uniform momentum zone observed close to the wall in Figs. 3a and 3b extends over more than one thousand viscous wall units along the streamwise direction. While it resembles the low speed streak that occurs in the buffer layer, it is a new and quite distinct phenomenon as it occurs well above the buffer layer and extends past the logarithmic layer [5]. However the low momentum zones are associated with near wall streaks, since the hairpin vortices and hairpin packets are believed to grow out of the near-wall streaks, at least in the first zone closest to the wall. The packets are also not the conventional bulges, but the largest packets in the hierarchy of hairpin packets might cause the bulges. The organization of the bulges appears to be less coherent than the packets, suggesting that the packets interact in a complex way.

3. Generation of hairpin vortex packets

The frequent occurrence of vortex packets in the experiments requires explanation. The kernel experiments of Acarlar and Smith [11, 12] followed the process of continuous generation of a train of hairpin vortices behind a hemispherical bump in a laminar boundary layer. Subsequent experiments by Haidari and Smith [13] considered the more relevant case of asingle hairpin vortex generated by an impulsive injection of fluid into the boundary layer and the subsequent generation of secondary hairpins to form a packet. This process of initial hairpin formation from fluid injection and its subsequent evolution and formation of additional vortical structures was studied numerically by Singer and Joslin [16]. Based on the experimental observations and inviscid computations, Smith *et al.* [17] offered a conceptual inviscid model for the mechanism by which new hairpins can be naturally generated out of a single hairpin. While the above cited investigations all pertain to the formation of a hairpin packet in a laminar boundary layer flow, the experimental evidence [5, 6, 8, 10] suggests that once a hairpin is formed by a localized, low momentum agency near the wall, it can, under a range of circumstances, proceed to generate a sequence of new vortices forming a coherent packet of hairpin vortices. A fundamentally similar general mechanism may occur in turbulent flow as well, but if so, it needs to be understood in that context.

The numerical simulations of the growth of a single hairpin vortex in the background of a low Reynolds number unidirectional mean turbulent channel flow [14, 15] offer additional insight into the mechanisms, which could explain the formation of new hairpin vortices, and their spatial arrangement into packets. These studies differ from the work described above in that the initial field was a viscous, hairpin vortex-like structure that was extracted from the full two-point turbulent correlation tensor of a $\mathrm{Re}_\tau = 180$ channel flow direct numerical simulation of Kim, Moser and Moin [18] by the process of stochastic estimation (*c.f.* Ref. 19), rather than created by external forcing. By appropriately choosing the event vector in the stochastic estimation process, the structure of the initial vortex can be varied over a wide range in a systematic manner to represent form an idealized symmetric hairpin to a more realistic asymmetric or one-sided hairpin.

Zhou *et al.* [14, 15] considered both symmetric and asymmetric Q2 event vectors given by a second quadrant velocity $[u = \alpha\sqrt{1-\beta^2}u_m,\ v = \alpha\sqrt{1-\beta^2}v_m,\ w = \beta(u_m^2 + v_m^2)^{1/2}]$ specified at a single point within the channel. Here (u_m, v_m) is chosen to maximize the product $u_m v_m$ weighted by the probability density of its occurrence $f(u_m, v_m)$ and thereby maximize the contribution to mean Reynolds shear stress. The factor α is a scaling factor, which determines the vortical strength of the initial structure relative to the vorticity of the mean flow. The factor β is the asymmetry parameter; $\beta = 0$ corresponds to a symmetric event and results in an initial symmetric hairpin. For a representative Q2 event, the stochastic estimation process guarantees that the initial field possessed the correct length scales, shape, and vorticity distribution of a typical Q2 structure. Thus we believe that the initial hairpin structure is more representative of the hairpin vortices observed in real turbulence.

Further, the background flow in which the hairpin vortex is embedded is chosen to be a unidirectional flow obtained from the mean streamwise velocity profile of $\mathrm{Re}_\tau = 180$ channel flow direct numerical simulation [18], rather than a Poiseuille flow. This difference at first glance might seem not so important; however, in the case of the turbulent mean flow profile the mean shear is predominantly contained close to the channel walls within approximately 25% of the channel half height ($y^+ < 45$), whereas in the case of a plane Poiseuille flow the mean shear extends over the entire channel. As a result the peak shear in the case of the mean turbulent profile is about factor four greater than that of the Poiseuille flow. A delicate balance between the self-induced velocity that tends to curl up the vortex and the influence of the mean shear, which tends to stretch the hairpin vortex, governs the evolution of the hairpin vortex. Thus differences in the mean background flow will have a strong influence on the dynamics of the initial hairpin vortex and the formation of the hairpin packet. In particular, the impact on the spatial and temporal scales of the resulting structure is likely to be strong.

In a real turbulent boundary layer the formation and evolution of the hairpin packet occurs in the presence of other hairpin packets, vortical debris, outer layer perturbations and so on. These disturbances are in deed collectively responsible for the mean turbulent profile, but of course in a time-averaged sense. The rational for using the unidirectional mean turbulent profile as the background flow is to account for the influence of the other turbulent structures at least in a statistical sense, and at the same time maintain the hairpin evolution simple and controlled so as to be able to follow it in close detail without any clutter from other vortical structures.

The simulations were performed at a Reynolds number of $\mathrm{Re}_\tau = 180$ in a box of streamwise (x) wall normal (y) and spanwise (z) size 4π, 2 and $4\pi/3$ respectively. The isosurface of the imaginary part of the eigenvalue of the velocity gradient tensor [15] is used to visualize vortices in the present study.

Time evolution of both symmetric and asymmetric initial structures were followed in detail with a direct numerical simulation. In both cases the quasi-streamwise vortices quickly lift away from the boundary due to mutual induction and the lift-up is the strongest at the downstream end. Simultaneously a shear layer forms where the Q2 velocity encounters the mean flow. Spanwise vorticity associated with this shear layer quickly rolls-up and forms a compact spanwise vortex located just above the downstream end of the quasi-streamwise vortices. By $t^+ \approx 25$ the rolled-up spanwise vortex viscously connects with the lifted quasi-streamwise vortices to form a hairpin structure. The geometry of this vortex resembles in appearance the hairpin vortices observed in many experiments. Fig. 4a shows the hairpin-like vortex at $t^+ \approx 27$ that resulted from an asymmetric initial structure with $y_m^+ = 30$, $\alpha = 2$ and $\beta = 0.5$. Apart from the hairpin vortex, marked by the head and an asymmetric pair of quasi-streamwise vortices on the upstream side of the hairpin head, a pair of vortical tongues can be seen on the downstream side of the head. These vortical tongues will later develop into new downstream hairpin vortices that will form part of the hairpin packet.

The head of the primary hairpin vortex continues to lift up into a near vertical orientation and also grows wider evolving into the characteristic Ω-shape. Simultaneously the quasi-streamwise legs stretch and form a kink as a result of mutual induction and interaction with the head. A shear layer forms above the kink and quickly intensifies. Subsequently the upstream portion of the quasi-streamwise legs detach from the primary hairpin at the kink and merge with the rolled up shear layer to form a secondary hairpin which remains distinct from the primary hairpin.

This process of new hairpin generation continues along similar lines both upstream and downstream of the primary hairpin resulting in a hairpin packet, which is shown in Figs. 4c and 4d at $t^+ \approx 144$. The envelope of the packet of hairpin vortices has a tent like appearance with an approximate angle of 10° upstream and 7° downstream of the primary vortex. The velocity signature of the computed hairpin packet qualitatively compares with the PIV measurements similar to those shown in Fig. 3. However discrepancies exist since the computed hairpins are separated along the streamwise direc-

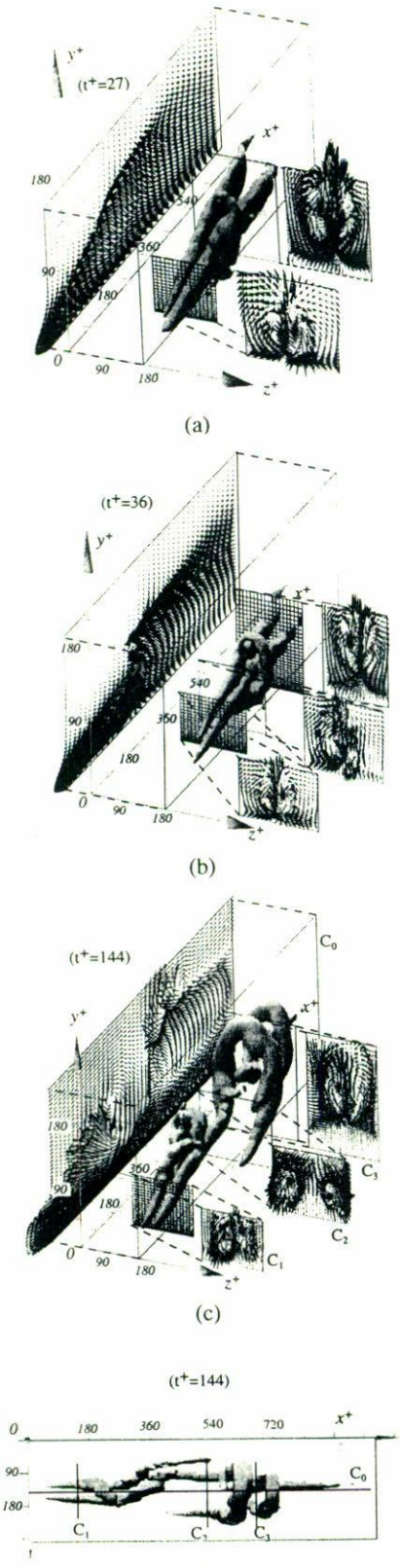

FIGURE 4. Hairpin packet that evolves from an asymmetric initial disturbance; (a) Perspective view, $t^+ = 27$; (b) Perspective view, $t^+ = 36$; (c) Perspective view, $t^+ = 144$; (d) Top view, $t^+ = 144$; (From Zhou *et al.* [15]).

tion about 200–450 viscous wall units, while in the experiments the distance between hairpins is observed to be around 100–150 viscous units.

The effect of asymmetry on the evolution of hairpin vortices is also investigated by systematically increasing the β parameter from 0. It is observed that the process by which new hairpins are autogenerated remains qualitatively the same as in the symmetric case. Thus the formation of a coherent hairpin packet is a robust mechanism active under a wide range of conditions. However, the asymmetric hairpins are one-sided and the packet consists of a streamwise train of alternating left and right handed one-sided hairpins that are staggered along the span. Both the symmetric and asymmetric cases display a threshold behavior; hairpins only above a certain threshold initial amplitude result in the autogeneration of new hairpins and formation of a hairpin packet. The threshold amplitude is observed to decrease with the degree of asymmetry suggesting that asymmetric hairpins are more likely to autogenerate and form hairpin packets than the idealized symmetric ones. This result is in total agreement with the experimental and computational observation of predominantly one-sided hairpins.

4. Single hairpin paradigm

Here we will consider significant experimental and computational observations that are consistent with the picture of the turbulent boundary layer populated with a forest of symmetric and cane-type hairpins.

1. The often observed quasi-streamwise vortices, hairpin shape and horseshoe (omega) shaped vortices, one-sided cane type vortices are all part of the same entity at various stages of their evolution and with different degree of asymmetry.

2. The range of hairpin vortex angle from 15°–75° (with 45° being more typical) is consistent with the range of angles observed from the quasi-streamwise vortices to the hairpin head. Furthermore, the tilt or angle of the hairpin head is a strong function of its location; the head takes a near vertical orientation in the outer regions of the boundary layer, while near the wall it takes a more conventional 45° angle.

3. The experimentally observed inclined internal shear layers can be explained on the basis of the Q2 fluid pumped by the hairpin encountering the free stream flow.

5. Hairpin packet paradigm

One must appeal to a coherent packet of streamwise aligned hairpin vortices in order to consistently explanation other experimental and computational observations of the past. Below we list all the important features that can be explained on the basis that the boundary layer is made up of hairpin packets.

5.1. Low-speed streaks

1. The cooperative Q2 pumping of the near-wall fluid by the streamwise aligned hairpin vortices explain the very long (more than 1000 wall units) low-speed streaks.
2. The spanwise staggering of the one-sided hairpins in the asymmetric case explain the often observed spanwise jogging of the low-speed steaks.
3. Recent measurements by Meinhart and Adrian [4] indicate that the low-speed streaks are not limited to the buffer-layer, but extend into the log-layer as well. Streamwise aligned hairpin vortices that extend into the log-layer, through their combined induced velocity can explain the long log-layer low-speed streaks.
4. The packet paradigm also explains the long tail observed in the u-correlation [20, 21].

5.2. Burst process

1. There is similarity to the POD results of Sirovich [22], in which the most important modes are the streamwise independent modes that hug close to the walls. These modes correspond to the streamwise aligned quasi-streamwise legs of the hairpins and the resulting long low-speed streaks. We interpret the propagating modes that trigger the onset of burst-like activity to be the projections of the hairpin heads.
2. The streamwise arrangement of the hairpin vortices is in agreement with the measurements of [23–25], where the near-wall burst process was observed to be typically made up of multiple Q2 events. In this sense the hairpin packet constitutes a burst.
3. The adjacency of hairpins within the packet results in strong internal shear layers where the induced downflow (Q4) from the upstream vortex head meets the low-speed upflow (Q2) induced by the downstream vortex. This Q2/Q4 stagnation point flow provides convincing evidence for the VITA signature, often used to identify burst process.
4. The conventional view of the burst process as wavy oscillation of the low-speed streaks and Q2 eruption at the end also fits into the framework of hairpin packet. While the low-speed (Q2) pumping of the downstream hairpins are somewhat mitigated by the corresponding Q4 induced velocity of their upstream neighbors, the low-speed pumping of the chronologically last upstream-most hairpin remains unopposed and in fact is reinforced by its downstream neighbors.

5.3. Structure and symmetry

1. Preference for cane-shaped one-sided hairpins in the experimental [1] and computational results [2] can be explained on the basis that the autogeneration of new hairpins is much more robust and readily occurring when they are asymmetric.
2. Often observed inline alignment of the streamwise vortices is due to the quasi-streamwise legs of the streamwise aligned hairpins within the packet.
3. In the event of strong asymmetry, only the alternative quasi-streamwise legs are significant—the packet is made up of alternating sequence of right and left handed canes. If one confines attention to only the near wall region ($y^+ < 60$) the behavior of the packet is very similar to that proposed by [26].

5.4. Hierarchy of packets

1. Recent PIV measurements [6] over a range of Reynolds numbers show velocity signature that is consistent with a picture of the turbulent boundary layer made up of hierarchy of hairpin packets that travel downstream coherently.
2. We believe that the hydrogen bubble measurements of [10] and the smoke visualizations of Head and Badyopadhyay [8] extract the near-wall and outermost groups of hairpins, respectively. This suggests the presence of hairpin packets right from the near-wall region to the outermost reaches of the boundary layer.
3. The outer scale structures such as the backs and bulges are consistent with a large-scale hairpin packet that extends into the outer layer.
4. The scaling of different quantities on inner, outer and mixed scales is compatible with the notion of a hierarchy of hairpin packets.
5. The smallest near-wall hairpin packet provides adequate explanation for the buffer-layer behavior. The nesting of smaller packets within larger ones, which are within even larger ones, and so on may explain the log-layer.
6. The hierarchy of packets can explain Robinson's observation that the buffer-region contains predominantly quasi-streamwise vortices, the log-region contains both quasi-streamwise vortices and hairpin heads and the wake-region contains mostly hairpin heads.

6. Implications of packet paradigm

Implications of the hairpin packet paradigm for prediction, control and modeling of turbulent boundary layer are very many. The superposition of the induced fields of the streamwise-aligned hairpins result in a strong Q2 velocity due to the "solenoid effect". This cooperative action leads to a potentially very large increase in momentum and heat transport from the wall. For example, the total Reynolds stress of N incoherently distributed (spatially uncorrelated) hairpin vortices is simply N times the individual contribution arising from the Q2 pumping of each of the hairpin. On the other

extreme, if the N hairpins are perfectly overlaid (perfect correlation) the resulting total Reynolds stress is N^2 times the individual contribution. The Reynolds stress contribution of a real hairpin packet is likely to scale somewhere in between and depend critically on the strength and spatial scales of the hairpin packet.

The above observation suggests that boundary layer models that are based on a hierarchy of random distribution of hairpins as in Perry *et al.* [3] have many of the ingredients necessary for an accurate description of the turbulent boundary layer, except for the coherence of hairpins within a packet. In a similar manner the phenomenological semi-Markov model of the turbulent boundary layer [27] does not fully account for the spatial coherence within the hairpin packet. By incorporating this important feature the predictive capability of these models can be significantly advanced.

Hairpin packets also provide exciting possibilities for the control of boundary layer turbulence and hence drag management. One simple conceptual approach to drag reduction is to delay the formation of secondary and subsequent vortices and thereby increase the streamwise spacing between the hairpins within the packet. The resulting reduced cooperation among the hairpins will significantly cut down the Reynolds shear stress and the momentum transfer. Recent results by Sirovich and coworkers [22] indicate that reasonable drag reduction can be achieved by random distribution of roughness elements.

They hypothesized that the roughness elements disturb the propagating modes and thereby control the bursting process. An alternative, but certainly related, viewpoint will be that the roughness elements adversely affect the hairpin generation process and mitigate the internal coherence within packets.

Experimental and computational evidence [11–16] suggests that many types of low momentum events at the wall can create a succession of hairpins. This along with [22] can be taken to suggest that by appropriate surface excitation, for example by momentum addition to overcome a local low momentum event the hairpin formation process can be controlled to reduce drag. Such exciting possibilities must be pursued in the future.

1. Y.G. Guezennec and W.C. Choi, in *Proc. Zoran P. Zaric Memorial International Seminar on Near Wall Turbulence, May 1988*, edited by S.J. Kline and N.H. Afgan, (Hemisphere, New York, 1989) p. 420.
2. S.K. Robinson, *Ann. Rev. Fluid Mech.* **23** (1991) 601.
3. A.E. Perry, S. Henbest, and M.S. Chong, *J. Fluid Mech.* **165** (1986) 163.
4. C.D. Meinhart and R.J. Adrian, *Phys. Fluids* **7** (1996) 694.
5. C.D. Meinhart and R.J. Adrian, (manuscript in preparation, 1998).
6. C.D. Tomkins, M.S. Thesis, University of Illinois, Urbana, Illinois, 1998.
7. T. Theodorsen, in *Proc. Second Midwestern Conf. of Fluid Mechanics*, (Ohio State University, Columbus, Ohio, 1952) p. 1.
8. M.R. Head and P. Bandyopadhyay, *J. Fluid Mech.* **107** (1981) 297.
9. P. Bandyopadhyay, *Phys. Fluids* **23** (1980) 2326.
10. C.R. Smith, "A synthesized model of the near-wall behavior in turbulent boundary layers", in *Proc. Eighth Symp.* on Turbulence edited by G.K. Patterson and J.K. Zakin, (University of Missouri-Rolla, Dept. of Chem. Engng., Rolla, Missouri, 1984).
11. M.S. Acarlar and C.R. Smith, *J. Fluid Mech.* **175** (1987a) 1.
12. M.S. Acarlar and C.R. Smith, *J. Fluid Mech.* **175** (1987b) 43.
13. A.H. Haidari, and C.R. Smith, *J. Fluid Mech.* **277** (1994) 135.
14. J. Zhou, R.J. Adrian, and S. Balachandar, *Phys. Fluids* **8** (1996) 288.
15. J. Zhou, R.J. Adrian, S. Balachandar, and T.M. Kendall, *J. Fluid Mech.* (1998) (submitted).
16. B.A. Singer and R.D. Joslin, *Phys. Fluids* **6** (1994) 3724.
17. C.R. Smith, J.D.A. Walker, A.H. Haidari, and U. Sobrun, *Philos. Trans. R. Soc. London, Ser. A* **336** (1991) 131.
18. J. Kim, P. Moin, and R.D. Moser, *J. Fluid Mech.* **177** (1987) 133.
19. R.J. Adrian, "Stochastic Estimation of the Structure of Turbulent Fields", in *Eddy Structure Identification*, edite by J.P. Bonnet, (Springer, Berlin, 1996) p. 145.
20. A.A. Townsend, *The structure of turbulent shear flow*, (Cambridge University Press, 1976).
21. H.L. Grant, *J. Fluid Mech.* **4** (1958) 149.
22. L. Sirovich, in *Self Sustaining Mechanisms of Wall Turbulence*, edited by R.L. Panton, (Computational Mechanics Publications, Southampton, UK) p. 333.
23. D.G. Bogard and W.G. Tiederman, *J. Fluid Mech* **162** (1986) 389.
24. T.S. Luchik and W.G. Tiederman, *J. Fluid Mech.* **174** (1987) 529.
25. F. Tardu, *Exp. Fluids* **19** (1995) 112.
26. J. Jeong and F. Hussain, *J. Fluid Mech.* **285** (1995) 69.
27. J.C.S. Meng, in *Self Sustaining Mechanisms of Wall Turbulence*, edited by R.L. Panton, (Computational Mechanics Publications, Southampton, UK) p. 201.